RESEARCH ARTICLE

NANO · MICRO small
www.small-journal.com

Catenation Control in Stable Zr-MOFs for Fine-Tuning LNG-ANG-Related Methane Storage

*Si Ma, Le Shi, Yuanlong Zhong, Honghao Cao, Zhenning Yang, Jian Yang, Kun Wang, and Zhijie Chen**

The liquefied natural gas and adsorbed natural gas (LNG-ANG) coupling systems are emerging as an attractive solution to solve boil-off gases generated by LNG tanks. Metal-organic frameworks (MOFs) are promising candidates for methane storage and delivery owing to their high porosity, large specific surface area, and tunable pore structures. However, systematically tuning LNG-ANG-related methane adsorption performance of MOFs has yet to be explored. In this context, an interpenetrated zirconium-based (3,8)-connected the-MOF, Zr-TTB-1, with limited porosity is synthesized. The further delicate modulation of reaction conditions allows the assembly of a non-interpenetrated counterpart, Zr-TTB-2, with significantly improved porosity. Such molecular-level catenation control results in a substantial increase in low-temperature methane adsorption performance related to LNG-ANG. The volumetric working capacity of non-interpenetrated Zr-TTB-2 is up to 255 cm^3 (standard temperature and pressure, STP) cm^{-3} under LNG-ANG condition (159 K, 6 bar, and 298 K, 5 bar), outperforms more than twice that of interpenetrated counterpart—Zr-TTB-1 (115 cm^3 (STP) cm^{-3}). To this end, the investigation provides an efficacious example of regulating the methane working capacity in LNG-ANG systems through molecular-level structural control of designed porous frameworks.

1. Introduction

The past few decades have witnessed rapid development of society and economy, but environmental issues, particularly the sharp upsurge in carbon dioxide emissions, caused by the massive use of fossil fuels are also increasingly troubling.[1] To achieve the goal of carbon neutrality, natural gas (NG), mainly consisting of methane, is considered a transitional fuel by virtue of natural abundance, low carbon-to-hydrogen ratio, and low distribution cost.[2] Compressed natural gas (CNG) requires special tanks and high pressures, thus limited to a special scope of utility because of potential safety concerns.[3] Liquefied natural gas (LNG) system has been commercialized, but the problem of boil-off gas (BOG) has yet to be resolved.[4] The emerging ANG technique, incorporating adsorbents, has attracted much attention due to conformable conditions, simple tanks, and convenient usage.[5] ANG often requires a long charging time to cool down when adsorbing a large amount of NG.[6] Recently, the coupling of LNG regasification and the ANG charging process, denoted as LNG-ANG coupling systems, are regarded as promising alternative to address the aforementioned troubles.[4,6] The LNG-ANG coupling strategy enables lower charging temperature than the traditional ANG process by heat exchange with the LNG regasification process. In this regard, high-efficiency adsorbents within LNG-ANG systems are key to adsorb BOG and then to reuse them.[4,6]

Metal-organic frameworks (MOFs) are a class of crystalline adsorptive materials assembled by organic linkers and inorganic metal nodes.[7] With merit of structural diversity, functional adjustability, high porosity, well-ordered framework, and abundant binding site, MOFs have emerged as ideal platforms for gas storage and separation, particularly methane storage.[8] Interpenetration, also expressed as catenation, is commonly occurrent in preparation of MOFs.[9] Interpenetration impacts the pore architectures, intrinsic properties, and functional application of MOFs.[10] For example, transient catenation in MOF significantly affects its uptake behavior for *n*-hexane,[11] while partially interpenetrated MOF possesses stepwise filling of pores thus obtains unique CO_2 isotherms.[12] In contrast, non-interpenetrated MOFs with high pore volumes and large surface areas are favorable for high methane storage capacity (**Scheme 1**). Zirconium-based MOFs (Zr-MOFs) are stable for many applications thanks to strong Zr-O coordination bonds and highly porous Zr-MOFs are known as outstanding adsorbents for gas storage.[13]

S. Ma, L. Shi, Y. Zhong, H. Cao, Z. Yang, J. Yang, K. Wang, Z. Chen
Department of Chemistry
Stoddart Institute of Molecular Science
Zhejiang Key Laboratory of Excited-State Energy Conversion and Energy Storage
State Key Laboratory of Silicon and Advanced Semiconductor Materials
Zhejiang University
Hangzhou 310058, P. R. China
E-mail: zhijiechen@zju.edu.cn

S. Ma, L. Shi, Y. Zhong, H. Cao, Z. Yang, J. Yang, K. Wang, Z. Chen
Zhejiang-Israel Joint Laboratory of Self-Assembling Functional Materials
ZJU-Hangzhou Global Scientific and Technological Innovation Center
Zhejiang University
Hangzhou 311215, P. R. China

The ORCID identification number(s) for the author(s) of this article can be found under https://doi.org/10.1002/smll.202409138

DOI: 10.1002/smll.202409138

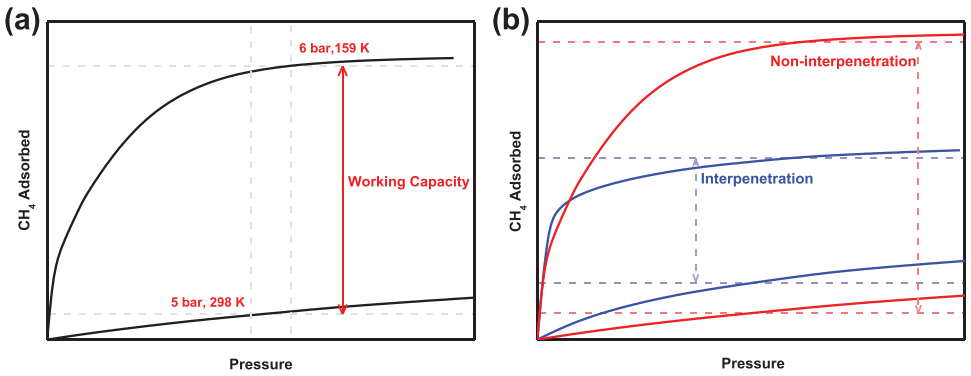

Scheme 1. a) The schematic diagram of working capacity between methane uptake at 159 K, 6 bar, and methane uptake at 298 K under 5 bar (LNG-ANG condition); b) The illustration of regulating methane sorption behavior by interpenetration control.

However, understanding deliberate interpenetration control in stable Zr-MOFs on gas storage, particularly low-temperature methane storage, has been rarely explored.

Herein, we provide a practical example of interpenetration control over stable Zr-MOFs for tuning low-temperature methane adsorption performance related to LNG-ANG applications. We first constructed a 2-fold interpenetrated Zr-MOFs (Zr-TTB-1) with limited porosity from newly-designed 5,5′,5′′-(benzene-1,3,5-triyl)tris(thiophene-2-carboxylic acid) (TTB) ligand. After careful optimization of reaction conditions, a non-interpenetrated counterpart—Zr-TTB-2 with greatly increased porosity was successfully prepared. The volumetric methane working capacity of non-interpenetrated Zr-TTB-2 (255 cm^3 (STP) cm^{-3}) is more than twice that of interpenetrated Zr-TTB-1 (115 cm^3 (STP) cm^{-3}) under the LNG-ANG-related condition (Scheme 1a), which is also comparable to those of typical HKUST-1 (249 cm^3 (STP) cm^{-3}) and MIL-101(Cr) (240 cm^3 (STP) cm^{-3}) under the same test condition.[6] Additionally, the gravimetric methane working capacity of Zr-TTB-2 is 0.26 g g^{-1}, significantly surpasses that of interpenetrated Zr-TTB-1(0.07 g g^{-1}). More importantly, the robust framework along with high porosity provide Zr-TTB-2 a great opportunity for practical implementation. The findings suggest that interpenetration control in MOFs is an attractive strategy to realize desirable methane working capacity in LNG-ANG systems, offering referenceable viewpoint on the development of the next-generation MOF-based absorbents for benchmark methane storage and delivery.

2. Results and Discussion

Zr-TTB-1 was synthesized with solvothermal reactions of TTB and $ZrCl_4$ in *N*,*N*-dimethylformamide with a modulator of acetic acid (HOAc) (**Figure 1**, left). Single-crystal X-ray diffraction (SCXRD) analyses reveal that Zr-TTB-1 crystallizes in the cubic space group $Im\bar{3}$ with the lattice parameter a = 25.9626(11) Å (Table S1, Supporting Information) at 273 K. The crystal structure of Zr-TTB-1 shows that each TTB linker is connected to three different Zr_6 clusters while each Zr_6 node is coordinated with eight carboxylic groups from eight different linkers (Figure S2, Supporting Information). The unsaturated sites in the Zr_6 clusters are occupied by three HOAc molecules and one formic acid (FA) molecule (Figure S5b, Supporting Information). Thus, we deduced the formula of Zr-TTB-1 to be $[Zr_6O_8(FA)_1(HOAc)_3(TTB)_{8/3}]$ as suggested by the ^{1}H NMR result of digested Zr-TTB-1 (Figure S8, Supporting Information). From the perspective of topology, the TTB linkers can be simplified as three connected nodes, which link to eight-connected Zr_6 clusters to generate a two-ford interpenetrated (3,8)-connected the-*c*2 net (Figure 2b; Figure S6, Supporting Information).[11,14] The phenomenon of structural interpenetration occurs in the preparation of MOFs by inducement of solvent, modulator, temperature, template, etc., therefore we assume that the formation of the two-fold interpenetrated Zr-TTB-1 could potentially be due to reaction conditions, ligand geometry, and the underlying the network.[9b,c]

To further increase pore volume and specific surface area, we aim to synthesize non-interpenetrated counterpart. Indeed, Zr-TTB-2 was formed under similar condition but modulated with trifluoroacetic acid (TFA) (Figure 1, right). The SCXRD analyses reveal that Zr-TTB-2 crystallizes in a cubic space group of $Pm\bar{3}$ with the lattice parameter a = 25.7367(14) Å (Table S2,

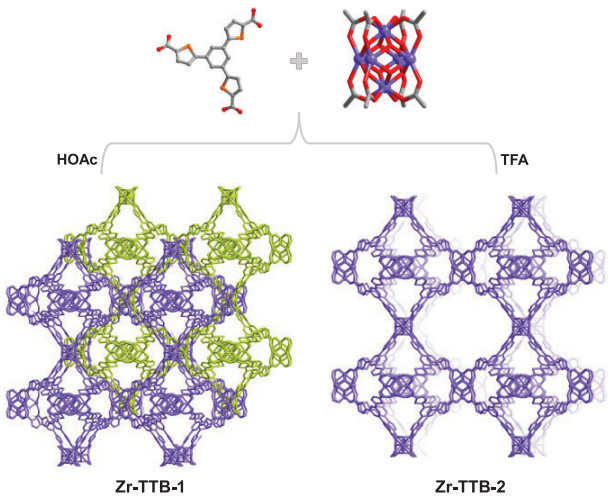

Figure 1. Structural illustration of Zr-TTB-1 and Zr-TTB-2. The construction of Zr-TTB-1 and Zr-TTB-2 from Zr_6 cluster and TTB ligand, modulated with acetic acid and trifluoroacetic acid respectively. Zr light purple, C gray, O red, S orange, and H atoms omitted for clarity.

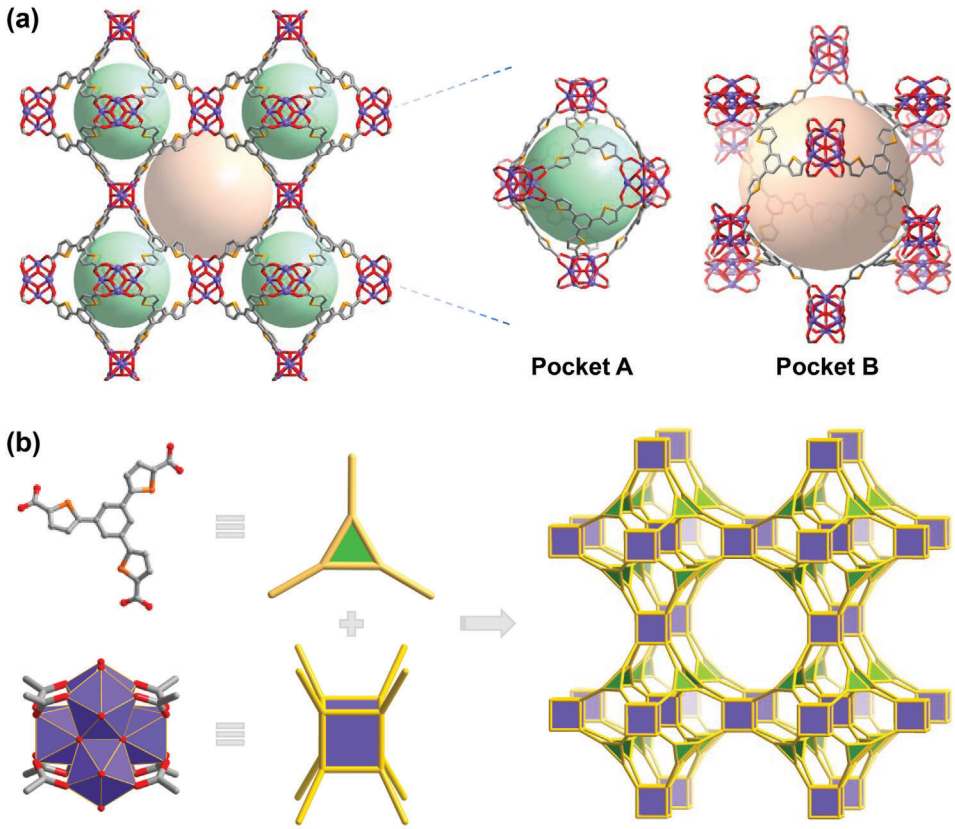

Figure 2. a) The schematic diagram of pockets in Zr-TTB-2; b) the topological diagram of Zr-TTBs. Zr light purple, C gray, O red, S orange, and H atoms omitted for clarity.

Supporting Information) at 273 K. Structurally, each TTB is connected to three different Zr_6 clusters, which function as nodes linking eight different TTBs (Figure S3, Supporting Information). Three TFA molecules and one FA molecule occupy the unsaturated sites in the Zr_6 clusters (Figures S4 and S5a, Supporting Information). The formula of Zr-TTB-2 is identified to be $[Zr_6O_8(FA)_1(TFA)_3(TTB)_{8/3}]$, further supported by the ^{1}H NMR and ^{19}F NMR experiment of digested Zr-TTB-2 (Figures S9 and S10, Supporting Information). Moreover, the Zr-TTB-2 possesses two pockets, ≈11 Å diameter sodalite cages, and channels with a width of ≈20 Å (**Figure** 2a). In contrast, the Zr-TTB-1 only retain ≈11 Å diameter sodalite cages as a result of structural interpenetration (Figure S7, Supporting Information).

The phase purities of two bulk Zr-MOFs are proved by their well-matched experimental powder X-ray diffraction (PXRD) patterns with simulated PXRD patterns (**Figure** 3a). Scanning electron microscope images display that Zr-TTB-1 possesses the regular octahedron morphology (Figure S19, Supporting Information), while Zr-TTB-2 possesses the cube morphology (Figure S20, Supporting Information). Moreover, the permanent porosity of two Zr-MOFs is evaluated by N_2 adsorption-desorption isotherms at 77 K. Zr-TTB-1 shows type I isotherms, suggesting its microporous architecture because of structural interpenetration (Figure 3b).[11] The apparent Brunauer-Emmett–Teller (BET) surface area of Zr-TTB-1 is calculated to be 580 $m^2\ g^{-1}$, and the experimental total pore volume is estimated to be 0.29 $cm^3\ g^{-1}$ at P/P_0 = 0.9. In sharp contrast, the N_2 sorption isotherm of Zr-TTB-2 exhibits a step shape (Figure 3b).[14] The calculated BET surface area of Zr-TTB-2 is estimated to be 2000 $m^2\ g^{-1}$, and the experimental total pore volume is 1.0 $cm^3\ g^{-1}$ at P/P_0 = 0.95, well matched with its theoretical value of 1.07 $cm^3\ g^{-1}$. The thermogravimetric analysis of activated Zr-TTB-1 and Zr-TTB-2 suggest that their decomposition temperatures under air flow are ≈300 °C (Figure S21, Supporting Information)

Generally, interpenetration will endow MOFs robust framework, thus Zr-TTB-1 is indicative of good stability.[15] As for non-interpenetrated counterpart—Zr-TTB-2, its chemical stability is further assessed by exposure to aqueous solutions with pH values ranging from 1 to 11. The almost unchanged PXRD patterns of Zr-TTB-2 before and after treatment indicate its good hydrolytically stability (Figure 3c).[15] The thermal stability of Zr-TTB-2 is also investigated by N_2 adsorption isotherms activated at indicated temperatures, which demonstrates its thermal tolerance up to 240 °C (Figure 3d). Overall, the significant enhancement of porosity for stable Zr-TTB-2 over Zr-TTB-1 foreshadows improved performance in LNG-ANG-related applications.

Considering the advantages of LNG-ANG coupling technique for methane storage, we then evaluate the methane working capacity of two Zr-MOFs under LNG-ANG conditions, that is, adsorption at 6 bar and 159 K and desorption at 5 bar and 298

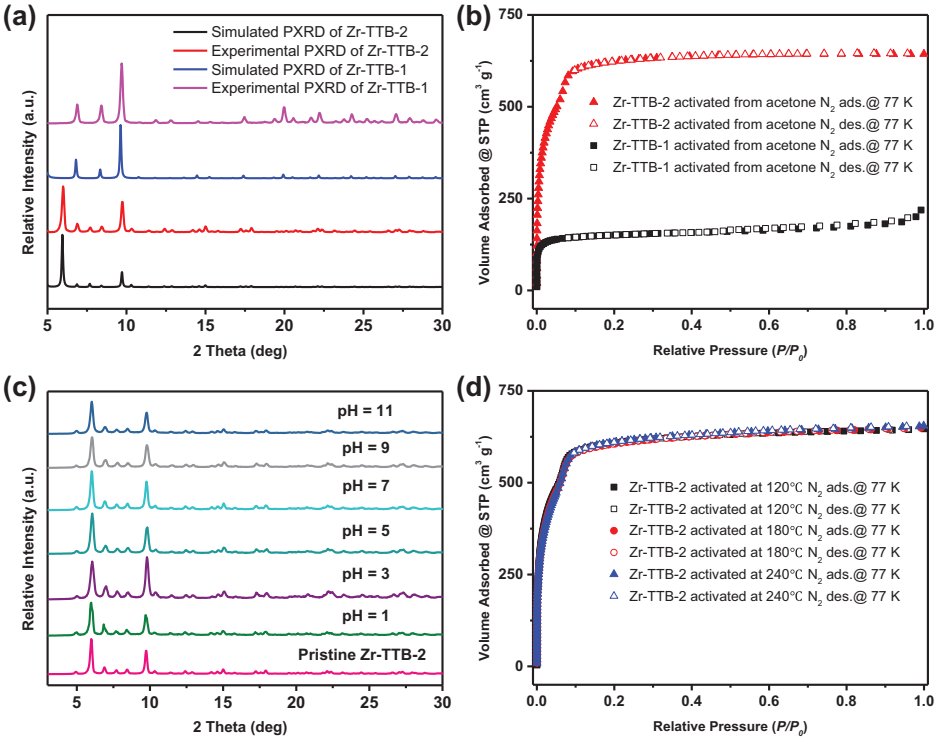

Figure 3. a) The experimental and simulated PXRD patterns of Zr-TTB-1 and Zr-TTB-2; b) Nitrogen sorption isotherm profiles of Zr-TTB-1 and Zr-TTB-2; c) PXRD patterns of Zr- TTB-2 after exposure to aqueous solutions with pH values ranging from 1 to 11; d) N_2 sorption isotherms profile of Zr-TTB-2 activated at different temperatures.

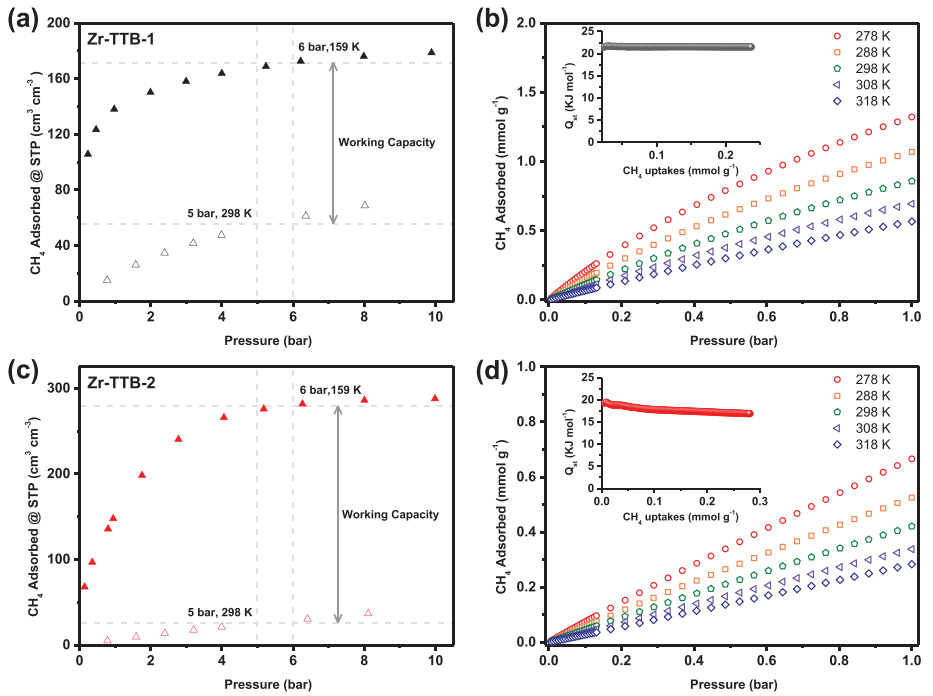

Figure 4. a) The volumetric sorption working capacity of Zr-TTB-1 between 5 bar, 298 K, and 6 bar, 159 K; b) The methane sorption of Zr-TTB-1 recorded at the indicated temperature, inset: Q_{st} for Zr-TTB-1; c) The volumetric sorption working capacity of Zr-TTB-2 between 5 bar, 298 K, and 6 bar, 159 K; d) The methane sorption of Zr-TTB-2 recorded at the indicated temperature, inset: Q_{st} for Zr-TTB-2.

K.[4,6] First, we investigate the effect of structural interpenetration on volumetric uptake of methane at 159 K (Figure S22, Supporting Information). Zr-TTB-1 exhibits a considerable uptake of methane at low pressure of 0.2–0.9 bar, but a slow increase of methane uptake as the pressure further increases. In contrast, Zr-TTB-2 shows a quick increase of methane uptake over the pressure range of 0.1–4 bar, and achieves a total volumetric methane uptake of 288 cm^3 (STP) cm^{-3} at 10 bar (Figure S22, Supporting Information).[16] Under LNG-ANG condition, the volumetric working capacity of Zr-TTB-2 is calculated to be 255 cm^3 (STP) cm^{-3} (**Figure 4a**), which is more than twice that of Zr-TTB-1 (115 cm^3 (STP) cm^{-3}, Figure 4c), indicating the successful realization of higher working capacity by suppressing structural interpenetration. The volumetric working capacity of Zr-TTB-2 also rivals those of classic HKUST-1 (249 cm^3 (STP) cm^{-3}) and MIL-101(Cr) (240 cm^3 (STP) cm^{-3}) under comparable conditions (LNG-ANG condition).[6] Moreover, the gravimetric working capacity of Zr-TTB-2 is up to 0.26 g g^{-1}, which is more than three times that of interpenetrated Zr-TTB-1(0.07 g g^{-1}) (Figures S25 and S26, Supporting Information).

In order to investigate the interaction effect between methane and Zr-MOFs, we deduced the isosteric heats of adsorption (Q_{st}) of two Zr-MOFs by fitting temperature-dependent methane isotherms using the virial method (Figure 4b,d).[17] The initial Q_{st} of Zr-TTB-2 is ≈19.2 kJ mol^{-1} (Figure 4d inset), which is slightly lower than that of Zr-TTB-1 (≈21.5 kJ mol^{-1}, Figure 4b inset), potentially due to the stronger interaction between the small-pore interpenetrated Zr-TTB-1 structure and methane.[18] In addition, the Q_{st} of two Zr-MOFs are slightly higher than those of classic HKUST-1 (17.0 kJ mol^{-1}),[18] UTSA-110a (14.5 kJ mol^{-1})[17c] and NOTT-102a (14.9 kJ mol^{-1}),[17c] and comparable to those of advanced MAF-38 (21.6 kJ mol^{-1})[17b] and Ni-MOF-74 (21.4 kJ mol^{-1}).[2a] Overall, Zr-TTB-2 exhibits excellent methane working capacity owing to robust framework, strong methane-adsorbent interaction as well as high population of accessible cages and channels via suppressing structural interpenetration.

3. Conclusion

In summary, a two-fold interpenetrated Zr-MOF with (3,8)-connected the topology, Zr-TTB-1, was constructed from newly-designed TTB ligand. In an effort to obtain larger porosity, a non-interpenetrated counterpart, Zr-TTB-2, was prepared via precise optimization. The two Zr-MOFs definitely exhibit great differences in pore volume, surface area, and methane adsorption performance. Under LNG-ANG condition, the volumetric working capacity of Zr-TTB-2 reaches to 255 cm^3 (STP) cm^{-3}, surpasses more than twice that of its interpenetrated counterpart—Zr-TTB-1 (115 cm^3 (STP) cm^{-3}). The volumetric working capacity of Zr-TTB-2 is also comparable to some classic MOFs, such as HKUST-1 and MIL-101(Cr). Additionally, the robust framework, high porosity and large surface area of Zr-TTB-2 as well as strong methane-adsorbent interaction render it promising for practical implementation. This work reveals the effect of subtle catenation control of MOFs on methane sorption behavior, also promotes the rational design of high-performance MOF-based absorbents at molecular level and the development of LNG-ANG coupling technique for efficient methane storage and delivery.

Supporting Information

Supporting Information is available from the Wiley Online Library or from the author.

Acknowledgements

Z.C. gratefully acknowledges support from the National Natural Science Foundation of China (grant no. 22471237, 22201247) and the startup funding from Zhejiang University. The authors thank the staff at BL17B1 beamline of the National Facility for Protein Science in Shanghai (NFPS), Shanghai Advanced Research Institute, CAS, for providing technical support in X-ray diffraction data collection and analysis. The authors thank the Chemistry Instrumentation Center at Zhejiang University for the technical support. This work was supported by the Leading Innovative and Entrepreneur Team Introduction Program of Zhejiang (No. 2023R01007).

Conflict of Interest

The authors declare no conflict of interest.

Data Availability Statement

The data that support the findings of this study are available from the corresponding author upon reasonable request.

Keywords

gas storage, interpenetration control, metal–organic frameworks, methane storage, zirconium-based MOFs

Received: October 24, 2024
Published online:

[1] a) M. Eddaoudi, J. Kim, N. Rosi, D. Vodak, J. Wachter, M. O'Keeffe, O. M. Yaghi, *Science* **2002**, *295*, 469; b) K. Sumida, D. L. Rogow, J. A. Mason, T. M. McDonald, E. D. Bloch, Z. R. Herm, T.-H. Bae, J. R. Long, *Chem. Rev.* **2011**, *112*, 724.
[2] a) Y. He, W. Zhou, G. Qian, B. Chen, *Chem. Soc. Rev.* **2014**, *43*, 5657; b) B. Li, H.-M. Wen, W. Zhou, J. Q. Xu, B. Chen, *Chem* **2016**, *1*, 557.
[3] G. Verma, S. Kumar, H. Vardhan, J. Ren, Z. Niu, T. Pham, L. Wojtas, S. Butikofer, J. C. Echeverria Garcia, Y.-S. Chen, B. Space, S. Ma, *Nano Res.* **2020**, *14*, 512.
[4] S.-Y. Kim, J. H. Kang, S.-I. Kim, Y.-S. Bae, *Chem. Eng. J.* **2019**, *365*, 242.
[5] a) K. Nath, K. R. Wright, A. Ahmed, D. J. Siegel, A. J. Matzger, *J. Am. Chem. Soc.* **2024**, *146*, 10517; b) S. Yang, Z. Zhong, J. Hu, X. Wang, B. Tan, *Adv. Mater.* **2024**, *36*, 2307579.
[6] S. Y. Kim, S. Han, S. Lee, J. H. Kang, S. Yoon, W. Park, M. W. Shin, J. Kim, Y. G. Chung, Y. S. Bae, *Adv. Sci.* **2022**, *9*, 2201559.
[7] a) L. Shi, Y. Zhong, H. Cao, H. Wang, Z. Xiong, K. Wang, H. Shen, Z. Chen, *Nat. Synth.* **2024**, https://doi.org/10.1038/s44160-024-00622-5; b) L. Shi, Z. Xiong, H. Wang, H. Cao, Z. Chen, *Chem* **2024**, *10*, 1; c) R.-B. Lin, S. Xiang, W. Zhou, B. Chen, *Chem* **2020**, *6*, 337; d) R.-B. Lin, S. Xiang, H. Xing, W. Zhou, B. Chen, *Coordin. Chem. Rev.* **2019**, *378*, 87.
[8] a) D. Alezi, Y. Belmabkhout, M. Suyetin, P. M. Bhatt, L. J. Weselinski, V. Solovyeva, K. Adil, I. Spanopoulos, P. N. Trikalitis, A. H. Emwas, M. Eddaoudi, *J. Am. Chem. Soc.* **2015**, *137*, 13308; b) P. Ajayan, W. Wang, Y. Chen, X. Bu, P. Feng, *Adv. Mater.* **2024**, *36*, 2408042; c) A. N. Hong,

H. Yang, X. Bu, P. Feng, *EnergyChem* **2022**, *4*, 100080; d) J. Li, P. M. Bhatt, J. Li, M. Eddaoudi, Y. Liu, *Adv. Mater.* **2020**, *32*, 2002563; e) H. Li, K. Wang, Y. Sun, C. T. Lollar, J. Li, H.-C. Zhou, *Mater. Today* **2018**, *21*, 108; f) Z. Chen, M. R. Mian, S.-J. Lee, H. Chen, X. Zhang, K. O. Kirlikovali, S. Shulda, P. Melix, A. S. Rosen, P. A. Parilla, T. Gennett, R. Q. Snurr, T. Islamoglu, T. Yildirim, O. K. Farha, *J. Am. Chem. Soc.* **2021**, *143*, 18838.

[9] a) R. Zhu, J. Ding, L. Jin, H. Pang, *Coordin. Chem. Rev.* **2019**, *389*, 119; b) M. Gupta, J. J. Vittal, *Chem. Rev.* **2021**, *435*, 213789; c) H.-L. Jiang, T. A. Makal, H.-C. Zhou, *Coordin. Chem. Rev.* **2013**, *257*, 2232.

[10] a) A. Ferguson, L. Liu, S. J. Tapperwijn, D. Perl, F.-X. Coudert, S. Van Cleuvenbergen, T. Verbiest, M. A. van der Veen, S. G. Telfer, *Nat. Chem.* **2016**, *8*, 250; b) D. Perl, S. J. Lee, A. Ferguson, G. B. Jameson, S. G. Telfer, *Nat. Chem.* **2023**, *15*, 1358; c) D.-J. Li, Q.-h. Li, Z.-R. Wang, Z.-Z. Ma, Z.-G. Gu, J. Zhang, *J. Am. Chem. Soc.* **2021**, *143*, 17162; d) M. Bonneau, C. Lavenn, J.-J. Zheng, A. Legrand, T. Ogawa, K. Sugimoto, F.-X. Coudert, R. Reau, S. Sakaki, K.-i. Otake, S. Kitagawa, *Nat. Chem.* **2022**, *14*, 816.

[11] L. Robison, X. Gong, A. M. Evans, F. A. Son, X. Wang, L. R. Redfern, M. C. Wasson, Z. H. Syed, Z. Chen, K. B. Idrees, T. Islamoglu, M. Delferro, W. R. Dichtel, F.-X. Coudert, N. C. Gianneschi, O. K. Farha, *J. Am. Chem. Soc.* **2021**, *143*, 1503.

[12] S. Yang, X. Lin, W. Lewis, M. Suyetin, E. Bichoutskaia, J. E. Parker, C. C. Tang, D. R. Allan, P. J. Rizkallah, P. Hubberstey, N. R. Champness, K. M. Thomas, A. J. Blake, M. Schröder, *Nat. Mater.* **2012**, *11*, 710.

[13] a) L. Shi, Z. Yang, F. Sha, Z. Chen, *Sci. China Chem.* **2023**, *66*, 3383; b) Z. Chen, K. O. Kirlikovali, L. Shi, O. K. Farha, *Mater. Horiz.* **2023**, *10*, 3257; c) Z. Chen, S. L. Hanna, L. R. Redfern, D. Alezi, T. Islamoglu, O. K. Farha, *Coordin. Chem. Rev.* **2019**, *386*, 32.

[14] B. Wang, X. L. Lv, D. Feng, L. H. Xie, J. Zhang, M. Li, Y. Xie, J. R. Li, H. C. Zhou, *J. Am. Chem. Soc.* **2016**, *138*, 6204.

[15] R. R. Liang, Y. Yang, Z. Han, V. I. Bakhmutov, J. Rushlow, Y. Fu, K. Y. Wang, H. C. Zhou, *Adv. Mater.* **2024**, *36*, 2407194.

[16] J. Tan, Y. Tao, X. Zhang, Q. Wang, T. Zeng, Z. Shi, K. E. Cordova, Y. Lee, H. Liu, Y.-B. Zhang, *J. Mater. Chem. A.* **2021**, *9*, 24857.

[17] a) J. Jiang, H. Furukawa, Y.-B. Zhang, O. M. Yaghi, *J. Am. Chem. Soc.* **2016**, *138*, 10244; b) J. M. Lin, C. T. He, Y. Liu, P. Q. Liao, D. D. Zhou, J. P. Zhang, X. M. Chen, *Angew. Chem., Int. Ed.* **2016**, *55*, 4674; c) H. M. Wen, B. Li, L. Li, R. B. Lin, W. Zhou, G. Qian, B. Chen, *Adv. Mater.* **2018**, *30*, 1704792.

[18] Y. Peng, V. Krungleviciute, I. Eryazici, J. T. Hupp, O. K. Farha, T. Yildirim, *J. Am. Chem. Soc.* **2013**, *135*, 11887.